How Frequent is Precipitation over the Contiguous United States? Perspectives from Ground-Based and Spaceborne Radars

MARK SMALLEY

NASA Jet Propulsion Laboratory, California Institute of Technology, Pasadena, California

PIERRE-EMMANUEL KIRSTETTER

Advanced Radar Research Center, University of Oklahoma, and National Severe Storms Laboratory, Norman, Oklahoma

TRISTAN L'ECUYER

University of Wisconsin–Madison, Madison, Wisconsin

(Manuscript received 14 October 2016, in final form 15 March 2017)

ABSTRACT

High temporal and spatial resolution observations of precipitation occurrence from the NEXRAD-based Multi-Radar Multi-Sensor (MRMS) system are compared to matched observations from *CloudSat* for 3 years over the contiguous United States (CONUS). Across the CONUS, precipitation is generally reported more frequently by *CloudSat* (7.8%) than by MRMS (6.3%), with dependence on factors such as the NEXRAD beam height, the near-surface air temperature, and the surface elevation. There is general agreement between ground-based and satellite-derived precipitation events over flat surfaces, especially in widespread precipitation events and when the NEXRAD beam heights are low. Within 100 km of the nearest NEXRAD site, MRMS reports a precipitation frequency of 7.54% while *CloudSat* reports 7.38%. However, further inspection reveals offsetting biases between the products, where *CloudSat* reports more snow and MRMS reports more rain. The magnitudes of these discrepancies correlate with elevation, but they are observed in both the complex terrain of the Rocky Mountains and the relatively flat midwestern areas of the CONUS. The findings advocate for caution when using MRMS frequency and accumulations in complex terrain, when temperatures are below freezing, and at ranges greater than 100 km. A multiresolution analysis shows that no more than 1.88% of *CloudSat* pixels over flat terrain are incorrectly identified as nonprecipitating as a result of shallow showers residing the *CloudSat* clutter-filled blind zone when near-surface air temperatures are above 15°C.

1. Introduction

Reliable observations of the frequency, spatial distribution, and intensity of rainfall and snowfall inform local weather forecasts, offer an observational benchmark for both daily weather forecast and reanalysis model evaluation, and provide early warning of severe weather, flash floods, and landslides. Dependable reanalyses of basic elements of daily weather including surface temperature and soil water content are contingent on accurate ancillary precipitation products (Gottschalck et al. 2005). Perturbations in satellite-based precipitation inputs to hydrologic models result in large differences in modeled streamflow volume and evapotranspiration, especially for smaller streams and when the perturbations are spatially correlated (Nijssen and Lettenmaier 2004). Even light precipitation can also have broad implications for Earth's energy balance; latent heat released in warm rain may partially account for imbalances in observational estimates of atmospheric energy balance (L'Ecuyer et al. 2015). Precipitation has also been shown to influence the lifetime and brightness of maritime clouds that exert a strong influence on top-of-atmosphere radiation balance.

Observations of the occurrence of precipitation necessary for these applications are generally derived from one of three sources: surface gauge networks, ground-based radar networks, or satellites. The Next Generation Weather Radar (NEXRAD), for example, is a network of S-band Weather Surveillance Radar-1988

Corresponding author: Mark Smalley, mark.a.smalley@jpl.nasa.gov

DOI: 10.1175/JHM-D-16-0242.1

Doppler (WSR-88D) radar sites across the United States, its territories, and its military bases. NEXRAD offers reflectivity and Doppler velocity measurements with high sensitivity and spatial resolution, especially near the radar sites. The installation of WSR-88D radars comprising NEXRAD led to the creation of NCEP stage IV (Lin and Mitchell 2005), a gridded NEXRAD and surface gauge accumulation product covering the contiguous United States (CONUS) and spanning from 2002 to present. Because of its high spatial resolution, relatively long record, stringent quality manual control, and near full-CONUS coverage, stage IV is often used as a reference in comparison and evaluation studies of models and other observational precipitation products (Wu et al. 2012; Gourley et al. 2010; Tesfagiorgis et al. 2011; Lin and Hou 2012).

The coverage of ground-based radar networks is, however, limited over many land areas and over the global oceans. Spaceborne radars improve data availability while providing researchers with not only precipitation rate estimates, but also information about cloud and precipitation vertical structure. In 2006, the *CloudSat* platform carrying the Cloud Profiling Radar (CPR) was launched into a sun-synchronous orbit with the goal of contributing to synergistic observations with other instruments in the A-Train satellite constellation (L'Ecuyer and Jiang 2010) to advance our understanding of microphysical cloud and aerosol processes. The *CloudSat* CPR is the first W-band spaceborne radar, providing near-global retrievals of finescale precipitation occurrence (Haynes et al. 2009) and precipitation rate in both frozen (Wood et al. 2014) and liquid phases (Lebsock and L'Ecuyer 2011). Previous efforts to evaluate the *CloudSat* precipitation products are encouraging (Ellis et al. 2009; Berg et al. 2010; Norin et al. 2015), but further evaluations for observations over land are necessary. Of particular interest are consequences of omitting the surface clutter correction over land surfaces, which was not designed to estimate clutter in complex terrain (NASA 2007), leading to questions of *CloudSat* precipitation retrieval in mountainous areas.

Despite the growing use of stage IV and *CloudSat* precipitation products, Smalley et al. (2014, hereafter SM14) demonstrated large differences between their precipitation occurrence statistics. These differences were greatest during the cold months, during which time *CloudSat* reported far more precipitation when the near-surface air temperature was close to or below 0°C. Conversely, only about 2% of all scenes were reported as precipitating by stage IV and nonprecipitating by *CloudSat*, a proportion that was observed to be stable across geographic location and when the near-surface air temperature was greater than 0°C. This led the authors to speculate that occasions when stage IV reported precipitation and *CloudSat* did not were primarily due to combined effects of temporal mismatches between the hourly stage IV accumulations and the instantaneous *CloudSat* measurements. However, the analysis in SM14 did not fully explain other sources of biases and agreement between the satellite and surface-based precipitation datasets, for example, the effect of the NEXRAD beam height on the stage IV detections. As the beam travels from the WSR-88D radar site, its height above the ground generally increases with distance from the radar, owing to the combined effects of surface curvature, surface orography, and atmospheric refraction (Doviak and Zrnić 1993). In addition, radar sensitivity decreases with the square of the distance from the radar site. The combined effects of beam height and decreased beam density at long ranges suggest that surface radars should provide more reliable detections of precipitation nearer the radar. The lack of precise temporal matchups between the hourly stage IV and instantaneous *CloudSat* observations and the lack of explicit accounting for the influence of distance on the comparisons precluded the quantification of the sources of the discrepancies in SM14.

This study evaluates collocated observations of precipitation occurrence from *CloudSat* and an independent reference precipitation product derived from NOAA/National Severe Storms Laboratory (NSSL) Multi-Radar Multi-Sensor (MRMS; Zhang et al. 2011, 2016). The MRMS precipitation product provides highly quality controlled gridded precipitation rates at high spatial and temporal resolution to estimate this critical component of the Earth atmosphere system over the CONUS. The MRMS radar mosaic data employed here are derived from the same NEXRAD observations as stage IV but are presented at a much higher spatial and temporal resolution, affording a more detailed analysis of the strengths and weaknesses of the NEXRAD surface radars and W-band spaceborne radars. Additionally, MRMS products are processed uniformly for all measurements over the CONUS, and specific products are generated to permit targeting environmental and observational conditions where precipitation estimates are likely more trustworthy. Examples of these products include the height of the NEXRAD beam, surface elevation, and precipitation observations at varying spatial and temporal resolutions. Several of these products are investigated in this study. MRMS also benefits from surface rain gauge inputs and extensive quality control efforts. Direct comparisons of collocated MRMS and *CloudSat* observations therefore allow a detailed assessment of the limitations inherent to both surface-based radar observations (e.g., undetected precipitation

TABLE 1. List of available designations from *CloudSat* 2CPC precipitation discrimination "Precip_flag." This study designates all scenes labeled as rain certain, mixed certain, and snow certain as precipitating and others as nonprecipitating.

Clear	Rain possible	Rain probable	Rain certain	Snow probable	Snow certain	Mixed probable	Mixed certain	Uncertain
0	1	2	3	4	5	6	7	9

in cold temperatures, in the western United States where radar coverage is sparse, and near topography) and spaceborne W-band radar observations (e.g., tradeoff between false detections and missed shallow precipitation caused by a valid observation height of more than 1 km above the surface).

The goal of this work is to examine comparisons of MRMS and *CloudSat* observations to determine the causes and regime dependence of challenges of providing high-quality ground-based and spaceborne radar precipitation measurements. Weather systems across the CONUS exhibit a wide range of characteristics and occur across a broad spectrum of surface types, providing the necessary environmental diversity to expose the uncertainties in each product as well as to highlight areas of good agreement between them. This study quantifies the dependence of biases on a combination of environmental factors such as topography, seasonal variations, near-surface air temperature, and instrument/algorithm factors such as radar beam height, ground clutter, and sensitivity.

The precipitation products used in this study are documented in section 2, and section 3 presents the mean precipitation totals reported by *CloudSat* and MRMS. Section 4 analyzes the effects of various factors relevant to the performance of each sensor across the CONUS, while section 5 limits comparisons to selected regions that highlight the individual challenges unique to each sensing system. Section 6 presents a discussion of the results in the context of another gridded NEXRAD–gauge product, NCEP stage IV. Conclusions are presented in section 7.

2. Data

a. The CloudSat *precipitation product*

The *CloudSat* platform orbits in an 0130/1330 local time sun-synchronous low-Earth orbit as a member of the A-Train satellite constellation. Its only science instrument is the CPR, a nadir-pointing 94 GHz W-band radar with a ground footprint of about 1.3 km × 1.7 km, a vertical resolution of 240 m, and a minimum detectable signal of about −28 dBZ (Tanelli et al. 2008). The sensitivity and resolution of the *CloudSat* CPR (hereafter *CloudSat*) permit detailed analyses of cloud and precipitation vertical and horizontal structure on a near-global scale (between 82°S and 82°N).

The principal *CloudSat* precipitation occurrence product is 2C-PRECIP-COLUMN (2CPC), described in Haynes et al. (2009). When discriminating precipitation by phase and confidence, the *CloudSat* 2CPC algorithm accounts for the maximum tropospheric temperature, the cloud-base height, the maximum in-cloud reflectivity in the lowest cloud, and the reflectivity of the lowest noncontaminated atmospheric height. The resulting precipitation phase and confidence categories are presented in Table 1 and are detailed in Haynes et al. (2009) and SM14. As noted in SM14, one important consideration when using *CloudSat* over land is that precipitation discrimination occurs in the fifth range bin (1.00–1.50 km) above the surface regardless of terrain or atmospheric conditions (Fig. 1b). This is done to avoid contamination of the reflectivity profile by surface returns, which can affect the lowest five range bins above the surface (Tanelli et al. 2008) since the current [release 04 (R04)] product does not include a surface clutter correction like that employed over ocean surfaces. This introduces some additional uncertainty in *CloudSat* precipitation occurrence estimates, particularly in complex terrain.

As a consequence of its measurement height, *CloudSat* 2CPC may miss valley rain or thin orographic precipitation in complex terrain or very shallow precipitation events in flat terrain. This is evident in the results of Norin et al. (2015), who find the closest agreement between the snowfall estimates from the *CloudSat* 2C-SNOW-PROFILE dataset and the C-band Swedish national weather radar network (Swerad) when collocated observations are made between 46 and 82 km from the nearest Swerad station. At longer distances, the Swerad radars lose sensitivity and have an increased chance of overshooting low snow events. But nearer the radar, some Swerad snow events are shallow enough to be obscured in the clutter-filled lowest range bins of *CloudSat*, causing an underestimation of snowfall rates in these cases. In cases of heavy snow, it has been shown that *CloudSat* underestimates snow rates due to attenuation of the CPR beam by large particles but reports higher frequency of light snow than the NEXRAD-based snow rate product NMQ (Cao et al. 2014). However, Chen et al. (2016) showed that when collocated

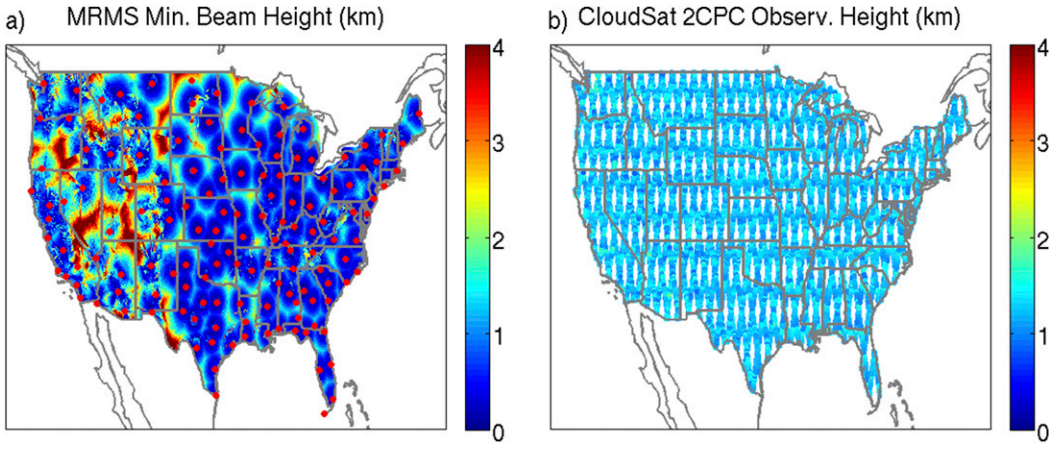

FIG. 1. (a) MRMS min beam height above the surface. (b) *CloudSat* 2CPC observation height above the surface.

comparisons were limited to conditions suitable for NEXRAD, snow occurrence from *CloudSat* is similar to snow occurrence from MRMS.

b. *The MRMS precipitation product*

MRMS integrates data from ground-based radar (NEXRAD, sites shown in Fig. 1a), automated rain gauge networks, and atmospheric model analyses in the CONUS and southern Canada to provide records of high-resolution (0.01°, 2 min) quantitative precipitation estimation (QPE) data over the CONUS. MRMS precipitation rates are used for many applications in hydrology (Gourley et al. 2017), evaluation of satellite QPEs (Kirstetter et al. 2014), and precipitation climatology studies (Zhang et al. 2016) and are available for assimilation in numerical weather prediction. MRMS mosaics radar reflectivity data onto a common 3D grid and estimates surface precipitation type, rate, and accumulations at different time scales. At each grid cell, the lowest altitude of nonmissing hybrid scan reflectivity comprising elevation angles closest to the surface values is recorded (Fig. 1a) to estimate surface precipitation. Coverage is best near populated areas with uniform terrain. Radar estimates are adjusted with rain gauge networks at hourly time steps. The 0.01° grid resolution of MRMS products provides great flexibility in matching MRMS samples to satellite footprints of choice (Kirstetter et al. 2012). Inspection of Fig. 1 reveals that NEXRAD beam heights are usually lower than the *CloudSat* measurement heights, except in areas with complex terrain or areas far from the nearest WSR-88D site. The MRMS precipitation product is limited in some areas by sparse NEXRAD and surface gauge coverage, beam blockage, and high beam heights in complex terrain, consistent with Maddox et al. (2002). In cases of beam blockage, MRMS precipitation estimation is performed by interpolation of surface gauge data, detections from other nearby radars, or the nearest radar at increased beam elevation angles (Zhang et al. 2011, 2016). Because of its complex terrain and frequent orographic precipitation, the mountainous western states provide challenging conditions to both spaceborne and surface-based precipitation radars.

c. *MRMS/*CloudSat *matchups*

This study employs direct matchups of selected precipitation-related *CloudSat* and MRMS, version 9, products. All areas observed coincidentally by *CloudSat* and MRMS were collected for the period from January 2008 to December 2010 (prior to NEXRAD dual-polarization upgrades). The MRMS products were matched in time to the *CloudSat* satellite local-overpass time. Spatially, the MRMS-derived precipitation was computed by averaging all MRMS pixels (precipitating and nonprecipitating) found within a specified radius around the center of the *CloudSat* footprint to compute unconditional mean rain rates at the *CloudSat* pixel scale. Three different scales are considered here:

1) Direct matchup: MRMS precipitation estimates using the 5-min MRMS products within a radius of ~1 km around the center of the *CloudSat* footprint. These spatiotemporal collocations allow direct comparisons between the two products to better understand the strengths and weaknesses of each observing system over the CONUS. Unless otherwise noted, the direct matchup MRMS dataset is used in comparison to *CloudSat* as it represents the closest spatiotemporal matchup.
2) Local area matchups: MRMS precipitation estimates at 5-min time resolution and 5-km spatial resolution to characterize the neighboring area.

3) Stage IV scale matchups: MRMS precipitation estimates at hourly time resolution and 5-km spatial resolution to match the resolution of NCEP stage IV.

In all, there are more than 7.2 million individual matched observations that contribute to this analysis. This study focuses on measurements of precipitation occurrence, as there is not yet an operational precipitation rate algorithm in release for land areas from *CloudSat*. *CloudSat* 2CPC pixels are considered precipitating if they satisfy any of the requirements of ''rain certain,'' ''snow certain,'' or ''mixed certain'' in the *CloudSat* database (Haynes et al. 2009; SM14). At a distance of 50 km from the nearest WSR-88D, radar echoes have been measured at -8 dBZ with a signal-to-noise ratio of 0 dB. However, the minimum detectable signal of individual radars at native resolution becomes less meaningful for a radar–gauge mosaic with individual scenes averaged to coarser resolution and often observed by multiple WSR-88D instruments. Therefore, any given MRMS native resolution (1 km, 2 min) location is considered precipitating if the mosaicked hybrid scan reflectivity is above 5 dBZ when the surface temperature is below 2°C and above 10 dBZ otherwise. The MRMS also employs a minimum detectable rain rate of 0.01 in. h^{-1} at the native ~1-km resolution, equivalent to about 0.25 mm h^{-1}. This threshold is applied prior to averaging and any pixels that have nonzero averaged rain rates are considered precipitating at each respective resolution.

3. Annual mean precipitation totals across the CONUS

Figure 2 compares precipitation maps at 2° resolution derived from the direct matchup MRMS (Fig. 2a) dataset and *CloudSat* 2CPC (Fig. 2b) between 2008 and 2010. While there is general agreement in the spatial pattern of precipitation events between the two datasets, *CloudSat* reports a relative 24% higher probability of precipitation (PoP) overall, and significant disagreements are evident over the western states in complex terrain. Figures 2c and 2d break the *CloudSat* precipitation in Fig. 2b down by phase, which is determined for overland scenes by a maximum tropospheric temperature from ECMWF of below 0°C for snow, between 0° and 2°C for mixed/uncertain, and above 2°C for rain (algorithm updated for overland scenes in SM14). The contribution of mixed/uncertain precipitation to Fig. 2d is small but generally follows the spatial pattern of the snow category (not shown). The map of *CloudSat* rain in Fig. 2c bears a close similarity

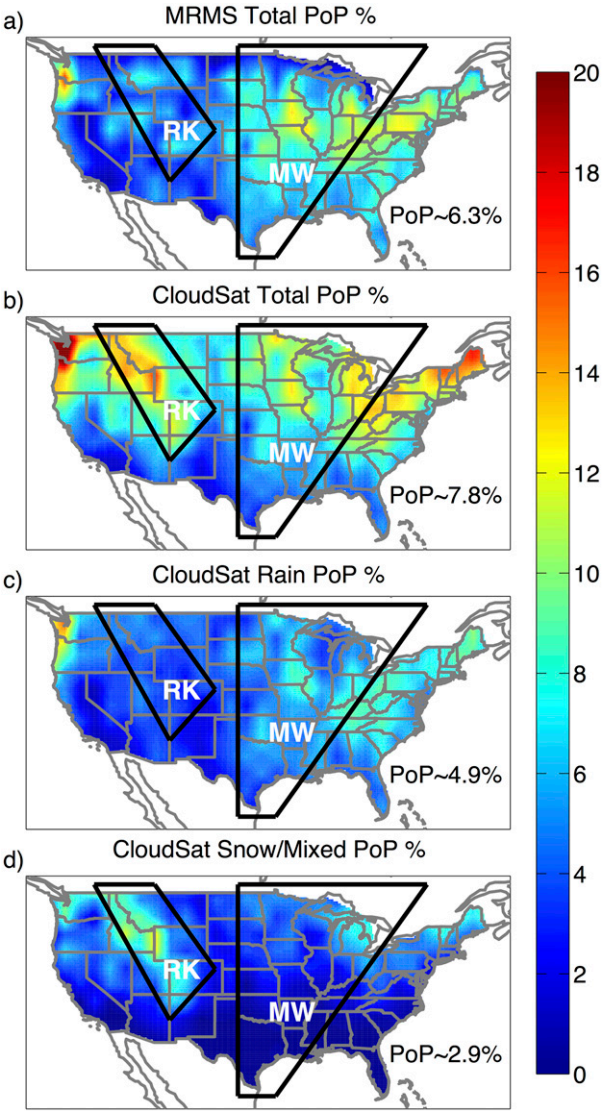

FIG. 2. Total PoP reported by (a) MRMS and (b) *CloudSat* 2CPC for matched observations from 2008 to 2010. *CloudSat* 2CPC observations from (b) are broken into phase as determined by *CloudSat* as (c) rain and (d) snow/mixed. Overlaid are black lines designating the RK and MW regions that are detailed in section 4.

to the MRMS totals in Fig. 2a, suggesting that frozen precipitation accounts for a significant portion of the disagreement in Figs. 2a and 2b. Figure 2d shows that much of the precipitation that *CloudSat* observes over the Rocky Mountains is reported as snow and that many of these cases are not reported by the MRMS. SM14 also documented significantly higher reported PoP from *CloudSat* than another NEXRAD-based retrieval (stage IV) in cold environments. This regime is examined more closely in section 4.

Also outlined in Fig. 2 are boundaries of the Rocky Mountains (RK) and Midwest (MW) regions, which

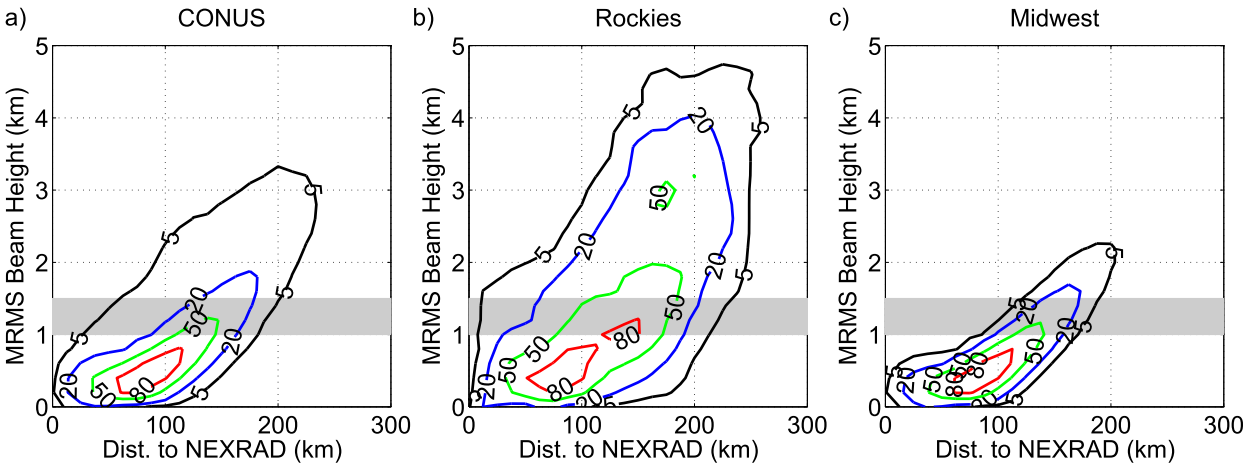

FIG. 3. Normalized frequency of MRMS beam height vs the distance to the nearest NEXRAD radar site for the (a) CONUS and the (b) RK and (c) MW regions defined in Fig. 2. Beam heights and distances are shown for collocated *CloudSat* 2CPC and MRMS pixels used in this study. Gray bars indicate the approximate *CloudSat* measurement height over land surfaces.

approximately capture major aspects of each observation environment and present unique challenges to the NEXRAD and *CloudSat* sensing systems. These regions represent relative extremes in terms of terrain variability, characteristic precipitation systems, and hydrologic concerns and also represent extremes in terms of the NEXRAD coverage uniformity and beam height in MRMS (Figs. 1a, 3). The WSR-88D beam height is a function of the distance from the nearest NEXRAD site, the scan elevation angle, and atmospheric refractive index (Doviak and Zrnić 1993). The flat terrain in the MW region results in a tight relationship between beam height and distance, but this tight relationship is broken over areas of complex terrain under beam blockage conditions, such as occur in the RK region. In the MW region (Fig. 3c), the NEXRAD beam height is a tight function of the distance to the nearest radar. On the other hand, complex terrain in the Rockies (Fig. 3b) forces the radar to sample at higher elevation angles, which increases the beam height compared to the MW region. The larger spread in beam height in the RK region highlights the greater diversity of observing conditions in complex terrain. Observations also tend to be made closer to the NEXRAD sites in the MW due to the more uniform and denser spatial coverage of NEXRAD sites in that region, which is beneficial when generating MRMS reflectivity mosaics.

A couple other areas of discrepancy merit brief mention. First, western Washington and Oregon are characterized by both frequent drizzle and complex terrain, leading to well-documented difficulties in observing precipitation with surface radars (Westrick et al. 1999). The upper northeastern states of Maine, New Hampshire, Vermont, and northern New York are also marked by large differences in total PoP. While beam heights are low in this area (Fig. 1a), nearly all the discrepancy can be attributed to observations made more than 100 km from the nearest NEXRAD site (not shown).

Figure 3 illustrates that the most frequent measurement height over CONUS is between about 0.3 and 0.7 km above the surface, which falls below the *CloudSat* measurement height of about 1.00–1.50 km. Thus, MRMS provides a more direct estimate of falling hydrometeors that actually reach the surface than *CloudSat* but also experiences an increased risk of false detections due to surface clutter at the lowest beam heights. While typical sources of ground clutter were largely mitigated even prior to the dual-polarimetric upgrade to NEXRAD, errors due to beam blockage (Lakshmanan et al. 2007) and biological sources (Lakshmanan et al. 2010) remained as significant challenges and a substantial effort is still made in MRMS to lessen the effects of these issues. See Zhang et al. (2016) for a detailed explanation of techniques used by MRMS to avoid surface clutter and biological radar echoes.

4. Role of geography, geometry, and the environment

The general depiction of how *CloudSat* and MRMS detect precipitation across the CONUS shown in Fig. 2 highlights broad similarities and differences between the products, but explaining their causes requires deeper analysis of how they vary as a function of specific environmental and geographic conditions. Such analyses may also help guide future algorithm improvements. Figure 4 compares *CloudSat* and MRMS precipitation

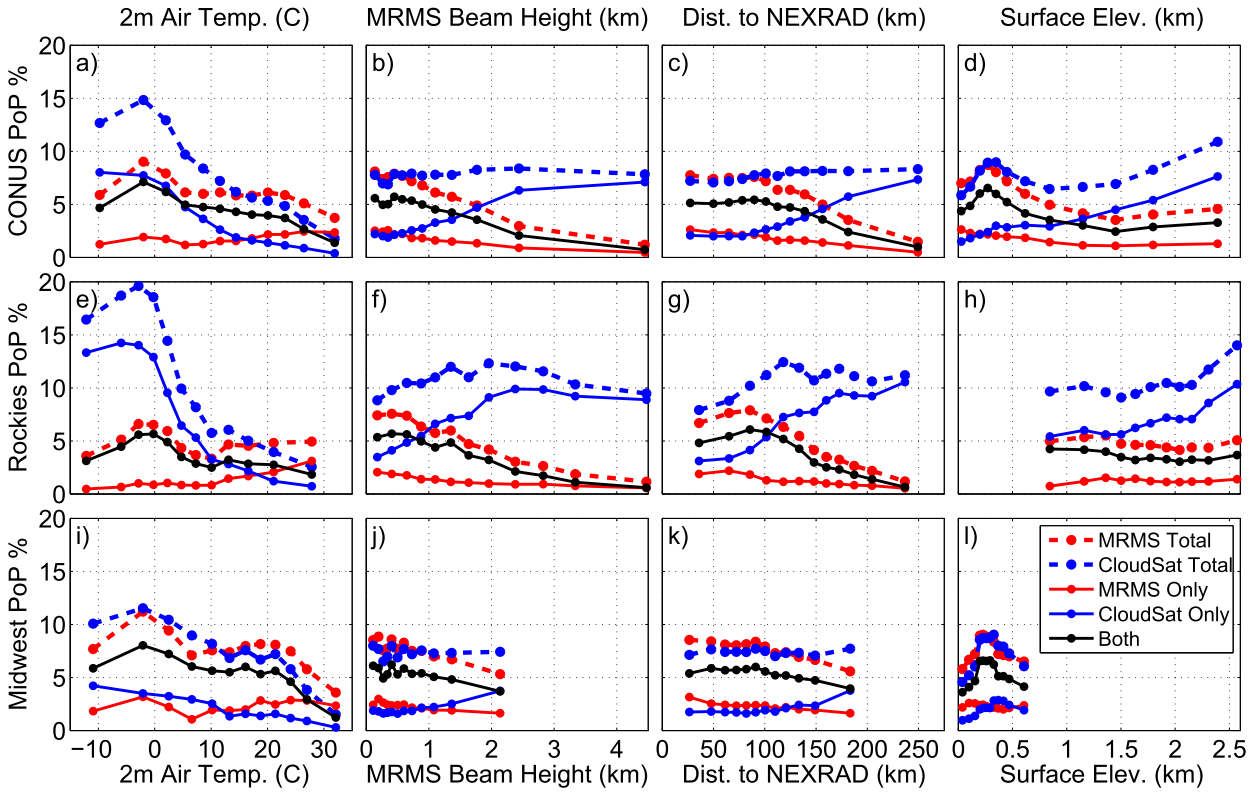

FIG. 4. Collocated *CloudSat* and MRMS PoP from the direct matchup dataset as a function of 12 quantiles of ECMWF 2-m air temperature, MRMS min beam height, distance to the nearest NEXRAD site, and surface elevation. Dashed lines show the totals observed by each product. The solid black line shows precipitation detected by both sensors. Solid red and blue lines show the precipitation exclusively detected by MRMS and *CloudSat*, respectively.

occurrence statistics from the direct matchups as a function of the near-surface air temperature from ECMWF, the height of the NEXRAD beam, the distance to the nearest NEXRAD site, and the surface elevation. Both sensors agree that precipitation is most frequent when near-surface temperatures are just below 0°C. However, *CloudSat* reports snow more frequently than MRMS in cooler environments while MRMS reports rain more frequently than *CloudSat* when near-surface air temperatures are above about 15°C (Fig. 4a). Figures 4e and 4i show that these discrepancies can largely be attributed to regional differences that persist into the broader CONUS statistics.

Close agreement is found between MRMS and *CloudSat* over the Midwest, except at the coldest and hottest temperatures. A majority of precipitation is observed by both sensors (solid black curve) while the number of events detected by only one sensor (red and blue curves) is relatively small. Conversely, a majority of the precipitation that falls at colder temperatures in the Rockies is observed only by *CloudSat* while a significant fraction of the precipitation falling at high surface temperatures is only observed by MRMS. Since colder temperatures are more frequently observed in the mountains and hot temperatures are more prevalent in the Midwest, this leads to regional biases between the datasets where MRMS observes more frequent precipitation at lower elevations and *CloudSat* observes more at higher elevations. This can be explained by examining Figs. 4b, 4f, and 4j and Figs. 4c, 4g, and 4k, which demonstrate that agreement is best in all regions when the MRMS beam is below about 1 km and when the matched observations are made within 100 km of the nearest NEXRAD site. This close agreement quickly fades as the observations are made farther from the NEXRAD site and as beam heights increase and radar sensitivity decreases. Much of the precipitation missed by MRMS at these distances is therefore likely shallow, light rain, or snow.

The substantial disagreement as a function of temperature in the Rockies region can be explained by a combination of the height of the MRMS beam, the distance to the nearest NEXRAD site, and surface elevation as shown in Figs. 4f–h. As NEXRAD beam heights increase far from their site sources in the Rockies region, MRMS PoP drops precipitously. In

Figs. 4f and 4g, *CloudSat* PoP appears to increase as a function of properties that should be independent of *CloudSat* observations. However, inspection of Fig. 4h in combination with Fig. 1a shows that the lack of NEXRAD coverage in the Rockies region is correlated with mountainous areas. Events that are generated or enhanced by orography are more difficult for MRMS to detect because of scant coverage. Since *CloudSat* observation heights are unaffected by complex terrain over land (Fig. 1b), it observes many more of these events, potentially explaining the increase in *CloudSat* PoP with increased distance from the nearest radar. Of course, these environmental properties are highly correlated and distinctions between their individual effects are difficult to express in this framework. When matched observations are made close to the NEXRAD sites, however, WSR-88D beam heights are lower than *CloudSat*'s fifth range bin, and MRMS measurements report an increasing amount of precipitation not detected by *CloudSat*. This suggests that *CloudSat* likely misses some very shallow events embedded in its clutter region.

Agreement is much closer in the MW region, even at temperatures below 0°C. This suggests that while precipitation phase might play a role in the discrepancy in the Rockies, temperature is not likely the only factor. Figures 4j–l show close agreement, with MRMS consistently reporting slightly higher PoP except when beam heights are at their highest farthest from the radar sites.

5. Regional analyses

To better illustrate the different detection capabilities of MRMS and *CloudSat*, the broad RK and the MW regions are analyzed separately. The complex terrain in the RK and the frequent snow and shallow rains in the MW present unique challenges to each observing system.

a. Influence of topography in the Rocky Mountains

Figure 5 shows bivariate distributions of total PoP and PoP exclusively detected by either instrument for the RK region as a function of temperature. When the near-surface air temperature is less than 0°C (cold regime), total MRMS detections (Fig. 5a) are associated with changes in beam height above the surface more than surface elevation. This is likely caused by a combination of a loss of sensitivity far from the NEXRAD radar site, the lowest beam elevation angles being blocked by complex terrain, and beam overshoot due to sparse radar coverage. On the other hand, total PoP reported by *CloudSat* (Fig. 5b) is mostly dependent on elevation. There is a strong similarity between MRMS total and both, illustrating that *CloudSat* generally agrees with MRMS when MRMS reports precipitation (i.e., infrequent MRMS only). The resulting *CloudSat* only exclusive detections (Fig. 5d) reflect the difference between the distributions in Figs. 5a and 5b, demonstrating that the differences between *CloudSat* and MRMS under these conditions depend both on elevation and NEXRAD beam height. The sample sizes are large and the results are smooth in each of the cold regime plots (Figs. 5a–e), adding confidence to this interpretation.

As temperatures increase to the cool regime ($0° < T < 15°C$), the sensors agree that precipitation occurs at lower elevations. The high agreement when MRMS detects precipitation follows this descent (Fig. 5j) and many of the times *CloudSat* reports precipitation but MRMS does not can be explained by high NEXRAD beam heights (Fig. 5i).

Figures 5k–m show analogous comparisons for the warm temperature regime ($T > 15°C$). In contrast to the cold and cool regimes, MRMS reports higher PoP than *CloudSat*. There is a distinct increase in PoP reported at high elevations by both *CloudSat* and MRMS (Fig. 5o). The ''hot spot'' in MRMS detections at elevations between 1.4 and 1.8 km and beam heights of less than 0.7 km is not observed in the *CloudSat* database, leading to questions concerning its validity. Closer inspection reveals that this feature is positioned in southeastern Wyoming (not shown). In the absence of this hot spot, general trends between MRMS and *CloudSat* are similar, with each reporting PoP increasing with both elevation and NEXRAD beam height.

Because *CloudSat* reports precipitation so frequently in the mountains, it is natural to suspect that the discrepancies are due to false detections due to surface clutter in the complex terrain. There is no guarantee that raising the observation height to the fifth bin above the surface is sufficient to avoid false detections from surface clutter. However, closer inspection adds confidence that the *CloudSat* detections in Fig. 5 are real for three reasons. First, it is not expected that the near-surface air temperature should be inversely correlated with the rate of *CloudSat* false detections, but there is a clear reduction in high-elevation PoP in Figs. 5g and 5i as the surface temperature increases. Actually, one can imagine that snowmelt mountain lakes and surface water would actually increase *CloudSat* false detections due to their flat, horizontal surfaces. Second, the increase in PoP reported by *CloudSat* in the warm regime (Fig. 5l) is corroborated by MRMS (Fig. 5k), which actually reports greater PoP at the highest observed elevations in warm temperatures. Also, MRMS reports the increase

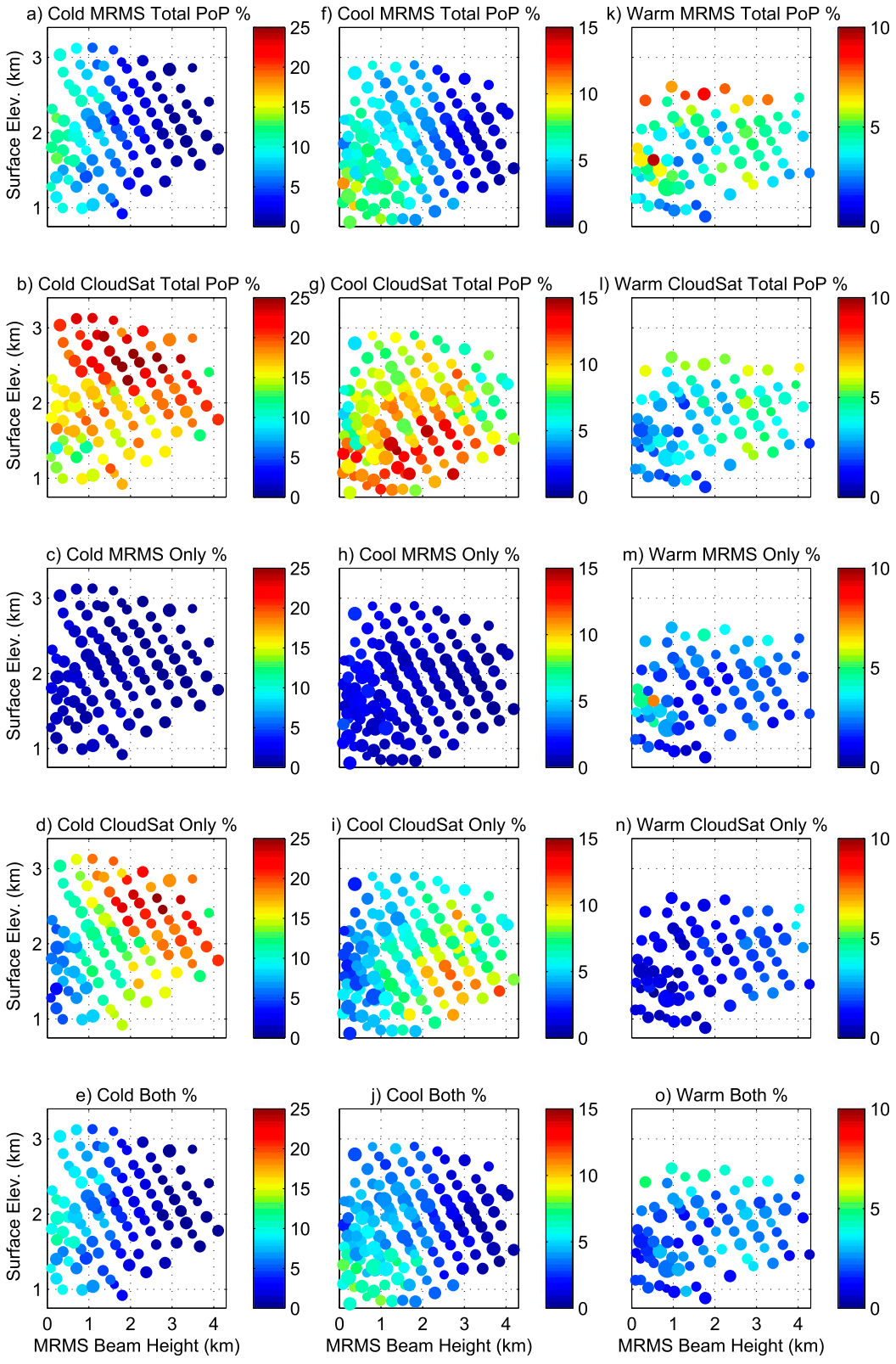

FIG. 5. Total and exclusive PoP reported by each dataset in the RK region illustrated by bivariate composites on surface elevation and MRMS beam height where (a)–(e), (f)–(j), and (k)–(o) designate the cold ($T < 0$°C), cool ($0° < T < 15$°C), and warm ($T > 15$°C) temperature regimes, respectively. Dot sizes are proportional to the number of observations contributing to each PoP estimate, where each estimate is composed of a min and max of 1500 and 6754 collocated observations, respectively.

in high-elevation PoP across a range of NEXRAD beam heights, indicating that the increase in MRMS PoP is not due to surface clutter. Mountain surface water is not expected to affect MRMS detections because NEXRAD views the atmosphere generally horizontally while *CloudSat* views it from above. Third, Mott et al. (2014) focused on orographic snow and demonstrated an enhancement of snow rate and occurrence near mountain peaks under synoptically driven events, corroborating the results in Fig. 5.

b. *Effects of MRMS resolution and proximity over the Midwest*

The central CONUS presents different challenges for efforts to remotely sense precipitation. Here, changes in elevation are relatively small and precipitation systems often propagate eastward as opposed to being geographically concentrated during their lifetimes. Figures 6a–c display detection statistics limited to the MW region outlined in Fig. 2, where PoP for the degraded resolutions of MRMS are shown in Figs. 6b and 6c. In contrast to the RK region, MRMS reports precipitation more frequently than *CloudSat* in the cold temperature regime when observations are made very near the NEXRAD radar sites. A recent study of shallow snow events from the *CloudSat* 2C-SNOW-PROFILE product suggests that some of the discrepancy close to NEXRAD sites (when beam heights are low; Fig. 3c) can be attributed to shallow cumuliform snow events embedded in the lowest *CloudSat* range bins (Kulie et al. 2016). However, as the distance to the nearest NEXRAD site increases beyond 100 km, the MRMS PoP falls quickly below PoP reported by *CloudSat*. Light rain and snow that occurs in the cool and cold temperature regimes becomes increasingly more difficult for the MRMS to detect as the beam diffuses far from the radar site.

To place these results in the context of the comparisons made in SM14 between *CloudSat* and stage IV precipitation occurrences at 60 min and 5 km scales, Fig. 6 also shows MRMS detections at local area matchup and at stage IV scale matchup resolutions as described in section 2. As the spatial and temporal resolutions of MRMS are degraded, higher PoP is reported. This is especially true near the NEXRAD sites, where beam heights are low and sensitivity is high. In this nearest quantile group, MRMS PoP increases 4.7% specifically due to increased search area (5 vs 2 km) between Figs. 6a and 6b and increases another 3.7% when the accumulation time is increased to an hour instead of 5 min between Figs. 6b and 6c. In a relative sense, the PoP increases the most in warm temperatures near the radar. In fact, PoP within 100 km of the nearest NEXRAD site is more than doubled when resolution is degraded to the stage IV scale matchup resolution. Clearly, it is important to account for resolution when utilizing precipitation occurrence statistics. Resolution has also been shown to be important for typology, rates, and the effects of nonuniform beam filling (Kirstetter et al. 2015).

In the MW warm regime, MRMS reports more frequent precipitation at all distances and resolutions. This could occur for a few reasons. Fast-moving or isolated convective precipitation generally occurs in warmer environments. In these cases, the increase in MRMS precipitation relative to *CloudSat* is most evident. It is important to remember that MRMS and *CloudSat* observations are built from instantaneous measurements and that those measurements can be made at any time during the collocated 5-min window, leading to instances in which a precipitation event exists within the collocated area when *CloudSat* passes overhead but not when NEXRAD makes its scan, contributing to *CloudSat* only. Note that degrading the MRMS spatial resolution to 5 km actually increases the agreement (both; Fig. 6h) until nearly all scenes reported by *CloudSat* are also reported by MRMS. This suggests that many of the instances of precipitation that are observed only by *CloudSat* at high resolution are due to these collocation mismatches. Increasing the accumulation period does not increase the agreement and merely adds to the amount of precipitation detected only by MRMS (MRMS only, Fig. 6i).

Another source of discrepancy is scenes where only part of one sensor's pixel is covered by precipitation, while more of the other sensor's pixel is filled. This partial beam filling has been shown to affect spaceborne radar precipitation retrievals (Tanelli et al. 2012; Kirstetter et al. 2015), but will be a factor in this study only when the edges of precipitating systems exist between the closely collocated MRMS and *CloudSat* footprints. This effect is indistinguishable from the temporal mismatch hypothesis at the 5-min resolution of these comparisons and so they are collectively referred to as fast moving/partial filling (FM/PF).

To test this temporal mismatch/rain system edge hypothesis, PoP from *CloudSat* and MRMS are composited against a benchmark of the local variability of precipitation occurrence surrounding each matched observation. Figure 7 shows the relationship between the warm regime matchups shown in Fig. 6g and deciles of the fraction of MRMS native-resolution (1 km) pixels that contain precipitation at the MRMS 5-km resolution (local area matchups). Doing so provides insights into the high-resolution spatial variability of precipitation occurrence during the matched observations. Averaging the MRMS data across all 10 deciles in Fig. 7 and

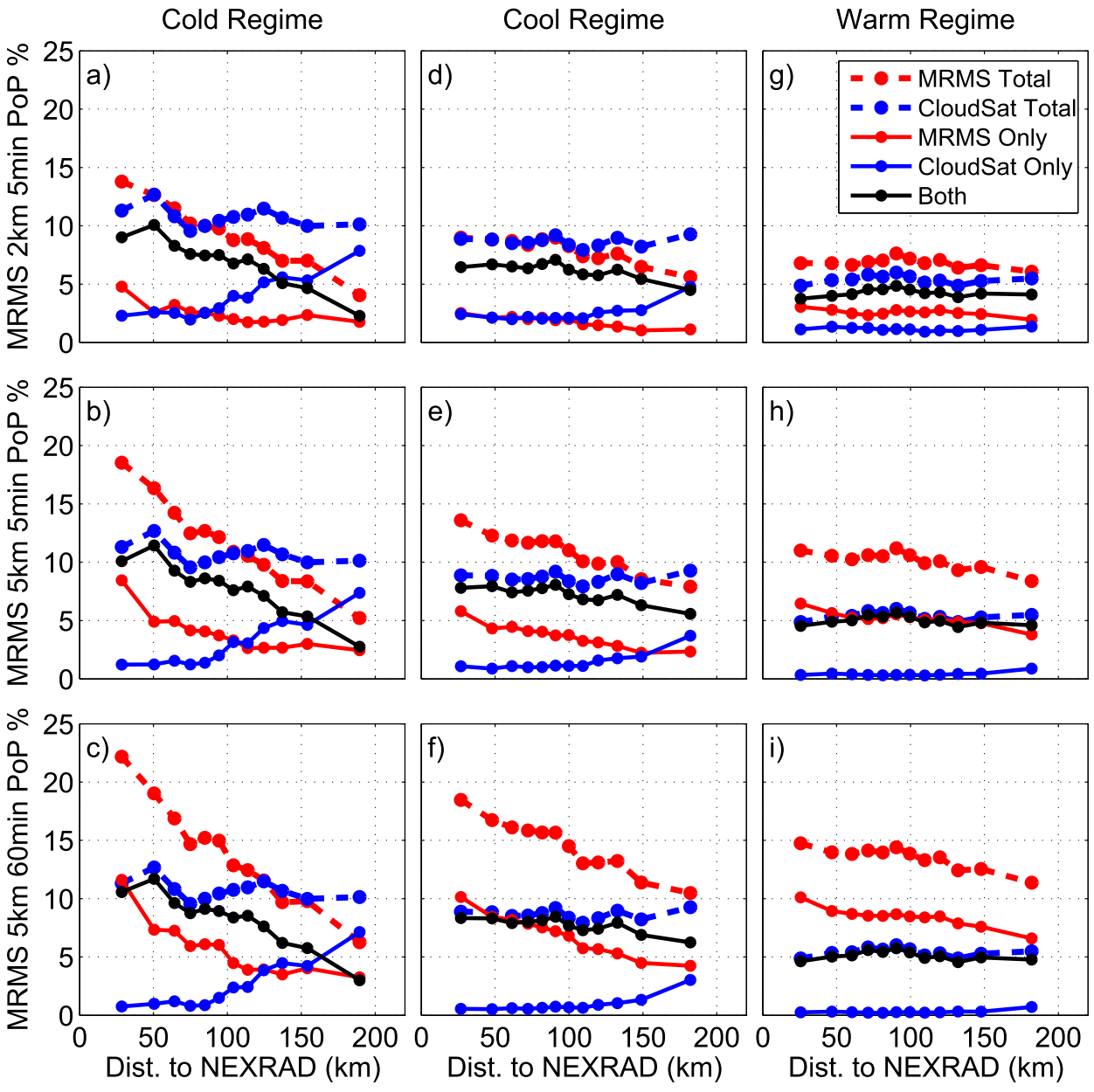

FIG. 6. As in Fig. 4, but for the distance to the nearest NEXRAD radar site and only covering the areas defined as the MW, as outlined in Fig. 2. Rows designate different MRMS spatial and temporal resolutions [(top) direct matchups, (middle) local area matchups, (bottom) stage IV scale matchups]. Comparisons have been separated into (left) cold ($T < 0$°C), (center) cool ($0° < T < 15$°C), and (right) warm ($T > 15$°C) temperature regimes by collocated ECMWF 2-m air temperature.

multiplying by the fraction of scenes where MRMS Precipitation Fraction (PF) > 0 gives the same overall precipitation fraction shown in Fig. 6g. The same is not true for the *CloudSat* data, as the *CloudSat* algorithm is permitted to report precipitation when the MRMS PF = 0. However, 91% of all *CloudSat* precipitating pixels occur when MRMS PF > 0 and therefore contribute to the *CloudSat* statistics in Fig. 7, demonstrating general agreement between the two precipitation products.

The greatest agreement (both category) occurs when MRMS reports precipitation across the full 5-km pixel. However, the discrepancy at MRMS PF = 1.0 shows that *CloudSat* is likely missing 10.9% of precipitation cases when MRMS is most confident of precipitation across the 5-km pixel. This adds to just over 3% of total collocated pixels in the MW warm temperature regime. It is unlikely that this discrepancy is due to MRMS false detections, as NEXRAD surface return signals do not

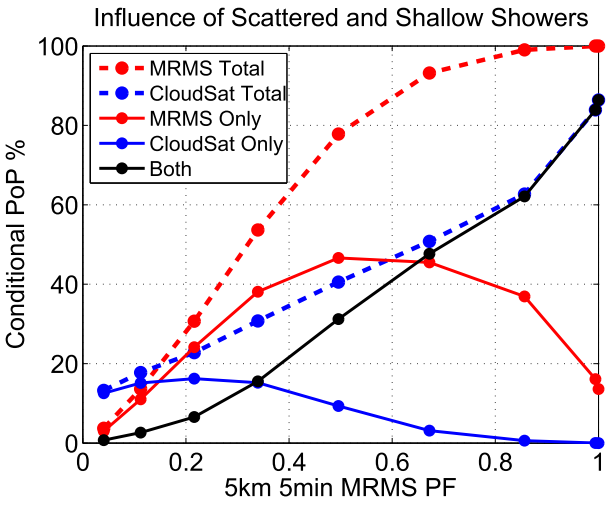

FIG. 7. As in Fig. 6g, but for results conditioned on the local area matchup (5 km, 5 min) MRMS PF. Pixels for which MRMS PF = 0 (90.1% of all pixels) are removed. The remaining data are composited into deciles of MRMS PF and the resulting conditional PoP for *CloudSat* and direct matchup MRMS (2 km, 5 min) data are shown. Because there are many instances of MRMS PF = 1.0, there are two overlapping deciles for each statistic at the MRMS PF = 1.0 and another decile visible at MRMS PF = 0.994.

typically cover a full 5-km pixel. Much of the discrepancy when MRMS is most confident must therefore be explained by very shallow rain events, as the NEXRAD beams are generally lower than the *CloudSat* observation height across the MW region (Fig. 1). However, these shallow events likely influence relative statistics when MRMS PF < 1.0 as well.

Differences between MRMS only and *CloudSat* only are most notable in Fig. 7 when the 5-km MRMS pixel is partially covered by precipitation (MRMS PF ≈ 0.65), suggesting that much of the disagreement in Fig. 6g can be attributed to FM/PF systems. Because shallow systems can be fast moving and scattered precipitation can fall from shallow heights, Fig. 7 cannot explain exactly which of the MRMS-only events are due to FM/PF rain and which are due to shallow rain. However, an estimation may be made based on observational characteristics of each platform, assumptions about the speed of propagating rain systems, and the inclusion of coarser-resolution MRMS precipitation detections.

Here, it is assumed that when comparisons are limited to conditions that are most suitable for surface radars, all existing rain is detected by MRMS. In this case, comparisons are limited to when NEXRAD beam heights are between 0.2 and 0.5 km in the Midwest warm temperature regime. Under these conditions, the only scenes reported as precipitating by *CloudSat* and not by MRMS in direct matchups must be a result of FM/PF showers, which are likely to be reported by MRMS in local area matchups. Because not all scenes observed in local area matchups truly passed over the central collocation area, it is also required that *CloudSat* observe precipitation. Therefore, the subtraction of *CloudSat* only in local area matchups from *CloudSat* only in direct matchups gives an estimate of the loss of MRMS PoP due to FM/PF systems. Because of the longer integration time in MRMS than *CloudSat* observations, this value (0.72%) also represents a lower bound of the effects of FM/PF systems on *CloudSat* detections in direct matchups. If these are the only two sources of missed detections under these conditions, the subtraction of this value from MRMS only in direct matchups yields an upper bound (1.88%) on how much PoP goes undetected by *CloudSat* due to shallow showers. Because WSR-88Ds make multiple scans during the 5-min window, the true value is likely much lower. The results are summarized in Table 2. The addition of *CloudSat* "rain probable" scenes to the analysis slightly reduces the effect of shallow showers, but also increases the risk of reporting false detections.

TABLE 2. Estimated PoP missed by *CloudSat* in the warm regime ($T > 15$°C) specifically due to shallow or fast moving/partial filling rain systems when compared to direct matchup MRMS at 2-km, 5-min resolution. The parentheses denote the values if *CloudSat* rain-probable scenes are considered as precipitating.

FM/PF (lower bound)	Shallow (upper bound)
0.72% (0.78%)	1.88% (1.74%)

Of course the validity of this hypothesis depends on an assumption that MRMS and *CloudSat* have comparable detection capabilities when precipitation truly exists during their respective instantaneous observations and that these are the only (or at least dominant) two sources of discrepancies under these conditions. It is seen from Fig. 6 that precipitation detections are most similar in this region and temperature regime than any other, suggesting that the assumption of comparable skill is satisfied. For this reason, a similar analysis is not possible for the Rocky Mountains, where there are clear detection differences between *CloudSat* and MRMS as a function of temperature (Fig. 4). This analysis also depends on the fast-moving systems missed by MRMS at direct matchup resolution being observed by MRMS at local area matchup resolution.

6. Discussion

The *CloudSat* and MRMS precipitation products each benefit from advantages unique to their observational and processing capabilities and offer high-quality estimates of rain and snow occurrence. Collocated observations show excellent agreement between these

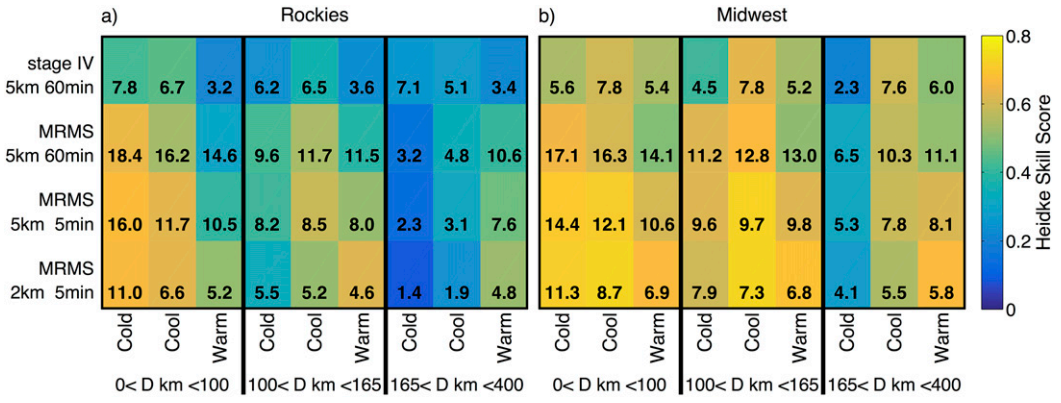

FIG. 8. HSS between *CloudSat* and NEXRAD-based stage IV and various MRMS resolutions in color for the (a) RK and (b) MW regions as a function of near-surface temperature regime and distance to the nearest NEXRAD site. NEXRAD-based total PoP is shown as text within each category for reference.

datasets when MRMS observations are within 100 km of the nearest radar site across the CONUS, consistent with previous works (Cao et al. 2014; Norin et al. 2015; Chen et al. 2016). However, the analyses also point to some inevitable observational challenges inherent to each platform. The comparisons identify three near-surface air temperature regimes, distinguished by 0° and 15°C, in which disparities between products depend on separate factors. Much of the minor disagreement over the Midwest in warm temperatures is found to be caused by quickly propagating or partially filling events, an unavoidable consequence of collocating instantaneous measurements over a finite temporal window. The remainder is estimated to be a result of shallow showers undetected by *CloudSat*. This proportion of *CloudSat* that missed PoP due to shallow showers in the warm regime (as well as the overall missed PoP) is reduced by considering rain-probable scenes as precipitating, but the impact is minor.

The results suggest that considerable caution should be exercised when using ground-based radar estimates to drive hydrologic models affected by cold season precipitation in complex terrain (Gourley et al. 2017). The quality of precipitation detection declines where intervening mountains inhibit low-level radar coverage, thus affecting snowpack and snow depth estimation and the snowmelt contribution to floods in meltwater runoff models. These models have been shown to be sensitive to precipitation inputs (Gottschalck et al. 2005; Nijssen and Lettenmaier 2004). While *CloudSat* does not provide sufficient temporal or spatial sampling to drive such models, its more uniform observation height, sensitivity, and calibration may provide a means for correcting for range effects in such applications.

CloudSat sometimes misses very shallow precipitation events that are embedded within its clutter region less than 1 km above the land surface. It is confidently stated that *CloudSat* misses no more than 1.88% PoP in warm environments over flat terrain due to shallow showers; the true value is likely to be much lower. In areas of uniform terrain (e.g., Midwest), 78.6% (69.5%) of all pixels identified as precipitating by *CloudSat* (MRMS direct matchups) are also identified as precipitating by MRMS direct matchups (*CloudSat*) resolution. It therefore appears that raising the observation height of *CloudSat* over land not only eliminates false positives in flat terrain but also causes the shallowest precipitation events to go undetected. However, many instances of pixels being reported by MRMS and not by *CloudSat* over flat terrain are the result of fast-moving, isolated convective events that preferentially add to MRMS detections to because of its multiple scans during the collocated time period. It should be noted that contributions of these fast-moving or partial-filling precipitation systems are significantly reduced compared to SM14, where NEXRAD-based stage IV detections are reported at hourly intervals.

To demonstrate the degree of agreement between *CloudSat* and MRMS and to provide additional context with the stage IV–*CloudSat* comparisons in SM14, Fig. 8 shows estimates of the Heidke skill score (HSS; Stephenson 2000) built from the 2×2 contingency table in Table 3 as a function of temperature regime and distance to the nearest NEXRAD site for comparisons between *CloudSat* and each of the considered MRMS resolutions. The HSS is defined here as Eq. (1), where the a, b, c, and d variables are set according to conditional detections outlined in previous figures. The HSS for collocated stage IV is also shown for context with SM14. For reference, the figure also displays the total PoP for each NEXRAD product at each distance and temperature regime:

TABLE 3. A 2 × 2 contingency table for yes/no binary flags from comparisons of *CloudSat* to MRMS and NCEP stage IV precipitation products. In this table, NEXRAD designates any choice of MRMS resolution or NCEP stage IV.

	CloudSat yes	*CloudSat* no
NEXRAD yes	a = both	b = NEXRAD only
NEXRAD no	c = *CloudSat* only	d = neither

$$\mathrm{HSS} = \frac{2(ad - bc)}{(a + c)(c + d) + (a + b)(b + d)}. \quad (1)$$

The HSS is an ideal skill score for this application because HSS = 0 for random forecasts and it is transpose symmetric (Stephenson 2000) and therefore does not hold preference for which precipitation product is the ''forecast'' and which is the ''observation'' in the 2 × 2 contingency table shown in Table 3. The HSS ranges from −1 to 1, with 1 representing perfect agreement and −1 representing perfect disagreement.

Overall, the high HSS in Fig. 8 indicates close agreement between *CloudSat* and various MRMS resolutions, most notably the direct matchups. As the MRMS spatial and temporal resolutions are degraded, the HSS generally decreases. Meanwhile MRMS total increases, as there are greater areas and time periods for which precipitation may occur at degraded resolution. It is clear from Fig. 8 that agreement between *CloudSat* and MRMS direct matchups is higher than between *CloudSat* and stage IV except at distances greater than 165 km in the cold and cool temperature regimes. Under these conditions, however, agreement with *CloudSat* is generally low for all NEXRAD products. It is also apparent that the precipitation observed exclusively by MRMS exhibits a greater dependence on temperature than that from stage IV, potentially resulting from automated homogeneous quality control in MRMS as opposed to manual and automated quality controls in stage IV.

7. Conclusions

The results of this study can be summarized as follows:

1) CONUS-wide PoP is 6.3% according to MRMS and 7.8% according to *CloudSat*. If *CloudSat* rain-probable scenes are also counted as precipitating, total PoP increases to 8.1% but the figures change only imperceptibly (not shown). MRMS and *CloudSat* precipitation statistics agree most closely near the NEXRAD sites where beam heights are low and when the terrain is uniform. These conditions are best suited for educated use of MRMS radar information in terms of resolution and quality.
2) When the near-surface air temperature is less than 0°C, the NEXRAD suffers from signal loss at locations far from the radar site and the resulting radar echoes fall below the threshold for detection of frozen precipitation, resulting in a reliance on sparse surface gauges. This is exacerbated in the Rocky Mountains, where *CloudSat* reports an increase in PoP with elevation when near-surface temperatures are below freezing, likely a result of orographic snow in the complex elevated terrain. This highlights the challenges for surface radars in snow events across the wide spectra of environmental regimes over the United States. These results are consistent with previous comparison studies between *CloudSat* and the Swedish operational radar network (Norin et al. 2015) and another NEXRAD-based precipitation product, NCEP stage IV (SM14), although agreement between *CloudSat* and MRMS is generally much higher than for *CloudSat* and stage IV.
3) When *CloudSat* reports precipitation in warm temperatures over flat terrain, MRMS almost always agrees. However, MRMS consistently reports precipitation more frequently than *CloudSat* under these conditions. Much of this discrepancy can be attributed to inevitable collocation mismatches. However, undetected shallow showers may affect up to 1.88% of *CloudSat* scenes over flat terrain in warm conditions, though the true value is likely much lower.
4) MRMS and *CloudSat* agree more closely than the stage IV–*CloudSat* comparisons presented in Fig. 8 and in SM14. Degrading the MRMS spatial and temporal resolution decreases agreement between MRMS and *CloudSat* (Fig. 8). This is especially true when temperatures are below freezing, indicating that the differences between stage IV and MRMS exclusive PoP extend beyond simple spatial and temporal resolution. Further study is required to understand specific differences between stage IV and MRMS quantitative precipitation products.

Acknowledgments. We are very much indebted to the MRMS and *CloudSat* teams responsible for providing these products. Thanks to Dr. Zac Flamig for his help in accessing the MRMS data used in this analysis. The MRMS precipitation product used here is version 9, with version 11 set to be processed soon. We also want to thank three anonymous reviewers, whose comments were very useful in improving the manuscript. The authors also acknowledge the support from the NASA-sponsored Jet Propulsion Laboratory, California Institute of Technology. M. S. and T. L. were supported by NASA *CloudSat*

Mission Grant NAS5-99237 and P. K. was supported by the NASA Grant NNX15AL36G. MRMS data can be found at http://mrms.ncep.noaa.gov/data/. The raw *CloudSat* 2C-PRECIP-COLUMN (2CPC) precipitation flags used in this study can be accessed from the *CloudSat* Data Processing Center at http://www.cloudsat.cira.colostate.edu/.

REFERENCES

Berg, W., T. L'Ecuyer, and J. M. Haynes, 2010: The distribution of rainfall over oceans from spaceborne radars. *J. Appl. Meteor. Climatol.*, **49**, 535–543, doi:10.1175/2009JAMC2330.1.

Cao, Q., Y. Hong, S. Chen, J. J. Gourley, J. Zhang, and P. Kirstetter, 2014: Snowfall detectability of NASA's *CloudSat*: The first cross-investigation of its 2C-SNOW-PROFILE product and National Multi-Sensor Mosaic QPE (NMQ) snowfall data. *Prog. Electromagnetics Res.*, **148**, 55–61, doi:10.2528/PIER14030405.

Chen, S., and Coauthors, 2016: Comparison of snowfall estimates from the NASA CloudSat Cloud Profiling Radar and NOAA/NSSL Multi-Radar Multi-Sensor System. *J. Hydrol.*, **541**, 862–872, doi:10.1016/j.jhydrol.2016.07.047.

Doviak, R., and D. Zrnić, 1993: *Doppler Radar and Weather Observations.* 2nd ed. Dover Publications, 562 pp.

Ellis, T. D., T. L'Ecuyer, J. M. Haynes, and G. L. Stephens, 2009: How often does it rain over the global oceans? The perspective from *CloudSat*. *Geophys. Res. Lett.*, **36**, L03815, doi:10.1029/2008GL036728.

Gottschalck, J., J. Meng, M. Rodell, and P. Houser, 2005: Analysis of multiple precipitation products and preliminary assessment of their impact on Global Land Data Assimilation System land surface states. *J. Hydrometeor.*, **6**, 573–598, doi:10.1175/JHM437.1.

Gourley, J. J., Y. Hong, Z. L. Flamig, L. Li, and J. Wang, 2010: Intercomparison of rainfall estimates from radar, satellite, gauge, and combinations for a season of record rainfall. *J. Appl. Meteor. Climatol.*, **49**, 437–452, doi:10.1175/2009JAMC2302.1.

——, and Coauthors, 2017: The FLASH project: Improving the tools for flash flood monitoring and prediction across the United States. *Bull. Amer. Meteor. Soc.*, **98**, 361–372, doi:10.1175/BAMS-D-15-00247.1.

Haynes, J. M., T. S. L'Ecuyer, G. L. Stephens, S. D. Miller, C. Mitrescu, N. B. Wood, and S. Tanelli, 2009: Rainfall retrieval over the ocean with spaceborne W-band radar. *J. Geophys. Res.*, **114**, D00A22, doi:10.1029/2008JD009973.

Kirstetter, P.-E., and Coauthors, 2012: Toward a framework for systematic error modeling of spaceborne precipitation radar with NOAA/NSSL ground radar-based National Mosaic QPE. *J. Hydrometeor.*, **13**, 1285–1300, doi:10.1175/JHM-D-11-0139.1.

——, Y. Hong, J. Gourley, Q. Cao, M. Schwaller, and W. Petersen, 2014: Research framework to bridge from the Global Precipitation Measurement mission core satellite to the constellation sensors using ground-radar-based National Mosaic QPE. *Remote Sensing of the Terrestrial Water Cycle*, *Geophysical Monogr.*, Vol. 206, Amer. Geophys. Union, 61–79, doi:10.1002/9781118872086.ch4.

——, ——, ——, and M. Schwaller, 2015: Impact of sub-pixel rainfall variability on spaceborne precipitation estimation: Evaluating the TRMM 2A25 product. *Quart. J. Roy. Meteor. Soc.*, **141**, 953–966, doi:10.1002/qj.2416.

Kulie, M. S., L. Milani, N. B. Wood, S. A. Tushaus, R. Bennartz, and T. S. L'Ecuyer, 2016: A shallow cumuliform snowfall census using spaceborne radar. *J. Hydrometeor.*, **17**, 1261–1279, doi:10.1175/JHM-D-15-0123.1.

Lakshmanan, V., A. Fritz, T. Smith, K. Hondl, and G. J. Stumpf, 2007: An automated technique to quality control radar reflectivity data. *J. Appl. Meteor. Climatol.*, **46**, 288–305, doi:10.1175/JAM2460.1.

——, J. Zhang, and K. Howard, 2010: A technique to censor biological echoes in radar reflectivity data. *J. Appl. Meteor. Climatol.*, **49**, 453–462, doi:10.1175/2009JAMC2255.1.

Lebsock, M. D., and T. S. L'Ecuyer, 2011: The retrieval of warm rain from *CloudSat*. *J. Geophys. Res.*, **116**, D20209, doi:10.1029/2011JD016076.

L'Ecuyer, T. S., and J. H. Jiang, 2010: Touring the atmosphere aboard the A-Train. *Phys. Today*, **63**, 36, doi:10.1063/1.3463626.

——, and Coauthors, 2015: The observed state of the energy budget in the early twenty-first century. *J. Climate*, **28**, 8319–8346, doi:10.1175/JCLI-D-14-00556.1.

Lin, X., and A. Y. Hou, 2012: Estimation of rain intensity spectra over the continental United States using ground radar–gauge measurements. *J. Climate*, **25**, 1901–1915, doi:10.1175/JCLI-D-11-00151.1.

Lin, Y., and K. E. Mitchell, 2005: The NCEP stage II/IV hourly precipitation analyses: Development and applications. *19th Conf. on Hydrology*, San Diego, CA, Amer. Meteor. Soc., 1.2. [Available online at https://ams.confex.com/ams/Annual2005/techprogram/paper_83847.htm.]

Maddox, R., J. Zhang, J. Gourley, and K. Howard, 2002: Weather radar coverage over the contiguous United States. *Wea. Forecasting*, **17**, 927–934, doi:10.1175/1520-0434(2002)017<0927:WRCOTC>2.0.CO;2.

Mott, R., D. Scipión, M. Schneebeli, N. Dawes, A. Berne, and M. Lehning, 2014: Orographic effects on snow deposition patterns in mountainous terrain. *J. Geophys. Res. Atmos.*, **119**, 1363–1385, doi:10.1002/2013JD019880.

NASA, 2007: Level 2 GEOPROF product process description and interface control document algorithm version 5.3. *CloudSat* Data Processing Center, 44 pp. [Available online at http://www.cloudsat.cira.colostate.edu/sites/default/files/products/files/2B-GEOPROF_PDICD.P_R04.20070628.pdf.]

Nijssen, B., and D. Lettenmaier, 2004: Effect of precipitation sampling error on simulated hydrological fluxes and states: Anticipating the Global Precipitation Measurement satellites. *J. Geophys. Res.*, **109**, D02103, doi:10.1029/2003JD003497.

Norin, L., A. Devasthale, T. S. L'Ecuyer, N. B. Wood, and M. Smalley, 2015: Intercomparison of snowfall estimates derived from the *CloudSat* Cloud Profiling Radar and the ground-based weather radar network over Sweden. *Atmos. Meas. Tech.*, **8**, 5009–5021, doi:10.5194/amt-8-5009-2015.

Smalley, M., T. L'Ecuyer, M. Lebsock, and J. Haynes, 2014: A comparison of precipitation occurrence from the NCEP stage IV QPE product and the *CloudSat* Cloud Profiling Radar. *J. Hydrometeor.*, **15**, 444–458, doi:10.1175/JHM-D-13-048.1.

Stephenson, D. B., 2000: Use of the "odds ratio" for diagnosing forecast skill. *Wea. Forecasting*, **15**, 221–232, doi:10.1175/1520-0434(2000)015<0221:UOTORF>2.0.CO;2.

Tanelli, S., S. L. Durden, K. S. Pak, D. G. Reinke, P. Partain, J. M. Haynes, and R. T. Marchand, 2008: *CloudSat*'s Cloud Profiling Radar after two years in orbit: Performance, calibration, and processing. *IEEE Trans. Geosci. Remote Sens.*, **46**, 3560–3573, doi:10.1109/TGRS.2008.2002030.

——, G. F. Sacco, S. L. Durden, and Z. S. Haddad, 2012: Impact of non-uniform beam filling on spaceborne cloud and precipitation

radar retrieval algorithms. *Remote Sensing of the Atmosphere, Clouds, and Precipitation*, T. Hayasaka, K. Nakamura, and E. Im, Eds., International Society for Optical Engineering (SPIE Proceedings, Vol. 8523), 852308, doi:10.1117/12.977375.

Tesfagiorgis, K., S. E. Mahani, N. Y. Krakauer, and R. Khanbilvardi, 2011: Bias correction of satellite rainfall estimates using a radar–gauge product: A case study in Oklahoma (USA). *Hydrol. Earth Syst. Sci.*, **15**, 2631–2647, doi:10.5194/hess-15-2631-2011.

Westrick, K. J., C. F. Mass, and B. A. Colle, 1999: The limitations of the WSR-88D radar network for quantitative precipitation measurement over the coastal western United States. *Bull. Amer. Meteor. Soc.*, **80**, 2289–2298, doi:10.1175/1520-0477(1999)080<2289:TLOTWR>2.0.CO;2.

Wood, N. B., T. S. L'Ecuyer, A. J. Heymsfield, G. L. Stephens, D. R. Hudak, and P. Rodriguez, 2014: Estimating snow microphysical properties using collocated multisensor observations. *J. Geophys. Res. Atmos.*, **119**, 8941–8961, doi:10.1002/2013JD021303.

Wu, W., D. Kitzmiller, and S. Wu, 2012: Evaluation of radar precipitation estimates from the National Mosaic and Multisensor Quantitative Precipitation Estimation system and the WSR-88D precipitation processing system over the conterminous United States. *J. Hydrometeor.*, **13**, 1080–1093, doi:10.1175/JHM-D-11-064.1.

Zhang, J., and Coauthors, 2011: National Mosaic and Multi-Sensor QPE (NMQ) system description, results, and future plans. *Bull.C Amer. Meteor. Soc.*, **92**, 1321–1338, doi:10.C1175/2011BAMS-D-11-00047.1.

——, and Coauthors, 2016: Multi-Radar Multi-Sensor (MRMS) quantitative precipitation estimation: Initial operating capabilities. *Bull. Amer. Meteor. Soc.*, **97**, 621–638, doi:10.1175/BAMS-D-14-00174.1.